17th AIAA/CEAS Aeroacoustics Conference (32nd AIAA Aeroacoustics Conference)
05 - 08 June 2011, Portland, Oregon

AIAA 2011-2888

17th AIAA/CEAS Aeroacoutics Conference, 6-8 June 2010, Portland, Oregon

A study based on the sweeping hypothesis to generate stochastic turbulence

Anthony Lafitte[*], Estelle Laurendeau[†]

Liebherr-Aerospace, 31016 Toulouse, France

Thomas Le Garrec[‡]

Onera - The French Aerospace Lab F-92322 Châtillon, France

Christophe Bailly[§]

Ecole Centrale Lyon, 69134 Ecully, France

With the development of so-called 'electric' aircraft, the integration of jet pumps to various systems of the engines could offer significant gains (mass, reliability,...) over the technologies currently used. Since jet pumps may directly contribute to ramp noise, an accurate predictive tool is therefore desired to propose adapted noise reduction solutions in an industrial context. A direct computation of the unsteady turbulent flow being too expensive, the main idea is to compute acoustic sources from a stochastic velocity field and to inject it in Euler's equations to model near-field acoustic propagation. A Kirchoff analogy is then used to reduce calculation cost in the far field. In following previous works by Bailly and Juvé (*AIAA Paper* 99-1872) and Billson *et al.* (*AIAA paper* 2003-3282), a combined approach to generate a stochastic velocity field is presented and validated in the present work. This methodology is based on the sweeping hypothesis - or the fact that small scale turbulent structures are advected by energy containing eddies. The validation study is done on aerodynamic quantities of a cold free jet at Mach number M=0.72. The capability of the method to reproduce space-time velocity correlations in the shear layer is shown. The model is then tested on a cold free jet configuration to predict radiated acoustic levels using a volumic Lighthill solver.

I. Introduction

Liebherr Aerospace Toulouse (LTS) develops air management systems designed for aircrafts. The function of such devices is to bleed high temperature, high pressure air from the engines, supply it to the cabin, condition it and then control its flow out of the cabin or circulate it along structural parts to be anti-iced. As part of the development of new designs responding to the emergence of so-called 'electric' aircraft, LTS works on the optimization of these air management systems and plans to integrate jet pumps which, for various functions of those systems, could offer significant gains (mass, reliability,...) over the technologies currently used. Practically, the jet pump can be considered as a simple jet confined in a duct, the ratio between the duct diameter and the nozzle diameter being about 5. Such a device, shown in Figure 1, may directly contributes to ramp noise. In order to propose appropriate noise reduction solutions, the use of a predictive tool for acoustics is required. In this study, a new method to generate acoustic jet sources is presented.

The common way to predict noise generated by the turbulent motions in the jet is to achieve a direct noise computation or to use hybrid methods. For the first approach - i.e a large eddy simulation (LES) or a direct numerical simulation (DNS) - a single calculation is needed to get both the flow and a part of the acoustic

[*]PhD Student, Computational Fluid Dynamics and Aeroacoustics Department, anthony.lafitte@onera.fr
[†]Research Engineer, Research and Expertise Department, estelle.laurendeau@liebherr.com
[‡]Research Engineer, Computational Fluid Dynamics and Aeroacoustics Department, thomas.le_garrec@onera.fr
[§]Professor, Senior Member AIAA, christophe.bailly@ec-lyon.fr

radiated field. Even with the rapid advances in computational capacities, these simulations are still too expensive to be applied in an industrial purpose involving complex configurations. Therefore, hybrid methods (CFD/CAA based approaches) can also be used for noise prediction. A first CFD simulation provides sources to be injected in a second calculation performed to obtain acoustics (an acoustic analogy for instance). The method presented in this paper is an hybrid one. Starting from the time-averaged flow quantities provided by a preliminary steady RANS solution, a stochastic velocity field is generated to build the acoustic sources. The radiated acoustic field is then recovered by a CAA approach. This RANS/CAA method should have the advantage of being less expensive in CPU than LES or DNS approaches. Note also that this approach should allow to take into account complex geometries without directly modelling correlation functions of turbulence, which is more difficult to do using statistical models.[1]

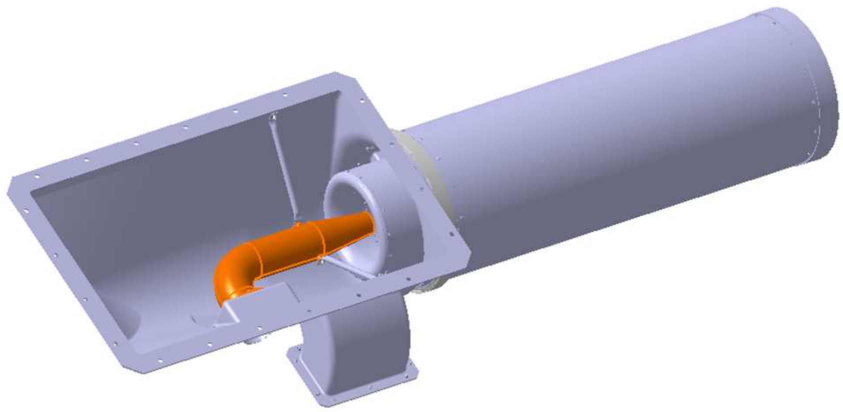

Figure 1. Scheme of the jet pump.

In the case of jet noise, or more generally of mixing noise, the turbulence modeling is one of the crucial point of the method. Since the early 70', many studies in various fields of application have dealt with stochastic methods. Interested in particle diffusion in incompressible, stationary and isotropic turbulence, Kraichnan[2] was the first to propose a method to generate a stochastic velocity field by considering a sum of Fourier modes. Since his former approach,[2] many methods have been formulated to compute such fields. Inspired by the work of Kraichnan,[2] the kinematic simulation (KS) is still widely used to study particle diffusion[3,4,5,6,7] in turbulent medium. Noticeably, Fung *et al.*[6] proposed an alternative version to the KS initial formulation by taking the sweeping effect - or the fact that the small scale vortices are advected by the energy containing eddies - into account. They introduced a separation between large and small scale velocity fields, the latter part being advected on the first one. Following the work of Karweit *et al.*[8] on the propagation of an acoustic wave through a turbulent medium, Bechara *et al.*[9] generate a stochastic velocity field for acoustic application. They proposed an approach by generating N pairwise independent realizations of the stochastic field constituted of spatial Fourier modes and considerating it as a temporal signal. Each local velocity signal field being random, the temporal coherence is then recovered by a temporal filtering of each local white noise. Bailly *et al.*[10] and later Bailly and Juvé[11] decided to take the convection effect into account directly in the stochastic field generation process. In practical terms, they added a convective term to Kraichnan's formulation[2] involving a convection velocity u_c which - and that was the big issue - had to be spatially constant to avoid a total decorrelation of the velocity field at large times. Billson *et al.*[12,13,14] resolved this problem by considering locally that the turbulent field was a superposition of a white noise and an advected term which is neither more nor less the turbulent field at the previous time step convected by the mean flow velocity. Later, they also included an anisotropy model proposed initially by Smirnov.[15] These Fourier modes formulations have been widely used[16,17,18,19,20] for acoustic applications. An other way to compute a turbulent velocity field is to filter a stochastic field spatially by a filter function built with the targeted space-time correlation function. Many formulations have been proposed to improve the former work of Careta *et al.*[21] who generated a stochastic field from a random stream function. On one hand, one can quote the development of the Random Particle Mesh method (RPM) by Ewert and Edmunds,[22] followed by Ewert[23] and its application to slat[24] and jet[25] noise. In the RPM, the streamlines are discretized regarding the time step and the local mean velocity of the flow. At each time step, the random particles - carrying the local stream function - located at each point of this grid are convected to the next point downstream before the advected random field is filtered. The resulting stream function mapping is then interpolated on the CAA grid and the turbulent velocity field is obtained locally by the rotational of the stream function. More recently, Ewert[23] noticeably reduced the computation cost of the RPM by restricting the number of particles used to compute acoustic source terms (Fast RPM). Siefert and Ewert[25] also studied the sweeping effect and its influence on sound generation in jets. On the other hand, the approaches based on a Langevin equation[26,27] can be classified in the same family of methods. Like for the RPM method, random particles carrying the stream function are placed along the streamlines according to the time step and the mean flow. In this case, the algorithm can be seen as a serie of convection and decorrelation steps. The convection is modeled in the same manner as for the RPM method and the decorrelation process is achieved applying a Langevin equation. Then, one can notice that stochastic methods are also used to generate inflow boundary conditions for various simulations, for instance at the interface between RANS and LES computations.[28,29,30]

A method combining on one hand the former idea of Fung *et al.*[6] about the sweeping effect, and on the other hand Bailly and Juvé[11] and Billson *et al.*[12] formulations, has been developed for the present work. The combined approach as well as results of its validation are presented in Section II. The validation study focuses on aerodynamic quantities since it is intrinsically linked to acoustic source terms. The validated method has then been tested on a free jet configuration. Section III shows acoustic results for the so-called Onera Φ80 free jet at Mach 0.72 ($U_j = 245$ m.s^{-1}) obtained by the coupling of the latter method and a volumic Lighthill solver.

II. Stochastic model

A. Presentation

In order to ensure a correct prediction of the acoustic radiation at the jet pump exit, the stochastic model must be able to generate a turbulent velocity field allowing the calculation of correct acoustic source terms inside the jet pump. Rubinstein *et al.*[31,32] showed that acoustic spectra are highly dependent on the space-time correlations. As a result, the hybrid model developed in the present work must be able to reproduce statistical aerodynamic quantities in the jet flow such as velocity space-time correlation functions. As well, it implies that the model - and it is not an easy task - correctly takes into account the convection velocity of the turbulent structures. Ideally, the method must be able to reproduce a turbulent kinetic energy map comparable to that given by the steady RANS simulation in order to keep a realistic spatial distribution of the most energetic acoustic sources.

The sweeping effect is known to be a fundamental decorrelation mechanism[6] and is suspected to play a crucial role in the sound generation process.[25] The method presented in this work to generate stochastic velocity fields is based on the sweeping hypothesis. It combines Bailly and Juvé[11] and Billson *et al.*[12] formulations. Following the idea of Fung *et al.*,[6] the turbulent velocity field $\mathbf{u}$ is separated into two parts respectively linked to the large (subscript l) and small (subscript s) scale structures:

$$\mathbf{u}(\mathbf{x}, t) = \mathbf{u}_l(\mathbf{x}, t) + \mathbf{u}_s(\mathbf{x}, t) \tag{1}$$

The starting point to build $\mathbf{u}_l$ and $\mathbf{u}_s$ is to impose locally an energy spectrum. In this case, the von Kármán-Pao spectrum which is adapted to homogenous isotropic turbulence is chosen. The equation (2) gives the expression of the von Kármán-Pao energy spectrum plotted in Figure 2 for a given $\overline{k}$ and ε.

$$E(k) = \alpha \frac{\overline{u^2}}{k_e} \frac{(k/k_e)^4}{[1 + (k/k_e)^2]^{17/6}} \exp\left[-\frac{3}{2} C_k \left(\frac{k}{k_\eta}\right)^{4/3}\right] \tag{2}$$

In equation (2), $k_\eta = (\varepsilon/\nu^3)^{1/4}$ is the Kolmogorov wave number, the Kolmogorov constant C_k is set to 3/2 and

$$k_e = \frac{0.747}{L} \tag{3}$$

with L the integral length scale set to

$$L = \alpha_f \frac{(\frac{2}{3}\overline{k})^{3/2}}{\varepsilon} \tag{4}$$

where α_f is a calibration factor. The separation between large and small scales is done by a cut-off wave number k_c as shown in Figure 2. Since the sweeping hypothesis corresponds to the advection of the inertial range turbulent structures by the energy containing eddies,[25] k_c is chosen locally to fall just after the spectrum maximum ($\approx 1.8k_e$). The energy spectrum is discretized linearly using a number N of spatial modes with k_n picked between a k_1 and a k_{max}. Since k_c is space dependent, the number of modes N_l and $N_s = N - N_l$ respectively linked to "large scale structures" and "small scale structures" vary spatially too. However, the wavenumber range is fixed for the whole computational domain. The choice of k_{max} is crucial. The more k_{max} is large, the more the energy injected from the von Kármaán-Pao spectra will be close to that given by the RANS calculation. In the present work, the reconstructed turbulent kinetic energy will be compared to that provided by the von Kármaán-spectra, assuming that increasing k_{max} - and then refining the mesh - will allow to obtain a $\overline{k}$ map similar to that of the steady computation.

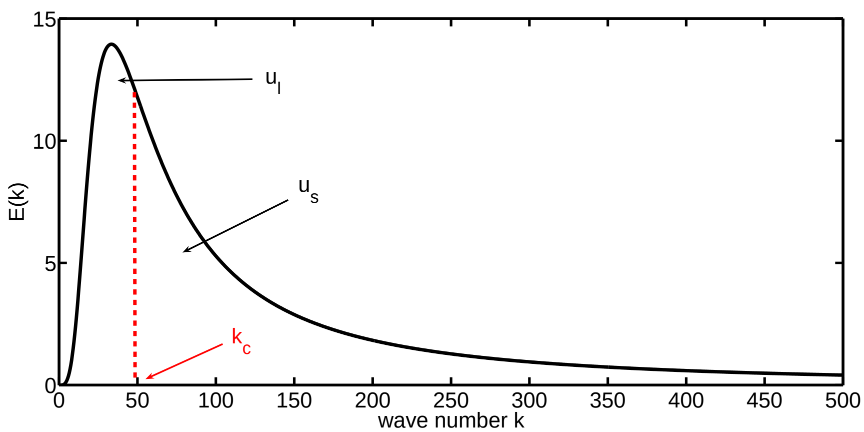

Figure 2. Generic von-Kármán-Pao energy spectrum showing separation between large and small scales.

The choice of the calibration factor α_f in equation (4) is not an easy task since it governs k_e and, therefore, the energy distribution among the Fourier modes. Experimentally, Fleury *et al.*[33] found that the longitudinal integral length scale in the shear layer is nearly equal to $2\delta_\theta$, with δ_θ the momentum thickness which can be approximated from the RANS computation. The Figure 3 shows the ratio between $2\delta_\theta$ and $(2/3\overline{k})^{3/2}/\varepsilon$, or in other words an approximation of the value of α_f along the shear layer. In the studied zone, this ratio is nearly equal to 1. Consequently, α_f is set to 1 for the present work.

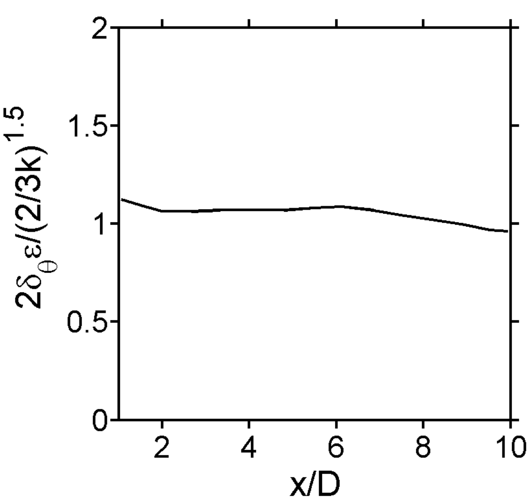

Figure 3. Calibration factor α_f at the center of the shear layer.

1. *Computation of the large scale velocity field $\boldsymbol{u}_l$*

Following the expression proposed by Bailly and Juvé,[11] the velocity field $\mathbf{u}_l$ associated to the large scale eddies is decomposed as a sum of N_l Fourier modes:

$$\mathbf{u}_l(\mathbf{x},t) = 2\sum_{n=1}^{N_l} \mathrm{A_n}\cos\left(\mathbf{k}_\mathrm{n}(\mathbf{x}-\mathbf{u}_\mathrm{c}t)+\omega_\mathrm{n}t+\varphi_\mathrm{n}\right)\boldsymbol{\sigma}_\mathrm{n} \tag{5}$$

with amplitude $A_n = \sqrt{E(k_n)\Delta k_n}$ built to conserve locally the turbulent kinetic energy imposed to the large scale structures. $\mathbf{k}_n$ and φ_n are respectively the wave vector and the phase of the nth mode. The direction $\boldsymbol{\sigma}_n$ satisfies the incompressibility hypothesis $\mathbf{k}_n \cdot \boldsymbol{\sigma}_n = 0$. Further explanations concerning the choice of these parameters are given in the litterature.[9,18] These Fourier modes are advected by a spatially constant convection velocity field $\mathbf{u}_c$ set to $0.6U_j$ in accordance with experiments.[33] ω_n stands for the temporal pulsation of the nth mode. In our case, the Kolmogorov pulsation defined by equation (6) is chosen since it is the most appropriate choice for low wave numbers[3] and it is known to give good results.[34,35] As remarked by Batten *et al.*,[36] if the convection velocity $\mathbf{u}_c$ and, in this case, the pulsations ω_n vary spatially, it automatically causes a total decorrelation of the turbulent velocity field at large times. A spatial mean value of the dissipation rate $<\varepsilon>$ is therefore used to calculate ω_n:

$$\omega_n = C_\mathrm{k}^{1/2} <\varepsilon>^{1/3} k_\mathrm{n}^{2/3} \tag{6}$$

The term $\mathbf{u}_l$ can therefore be explicitely formed at each time step of the numerical simulation.

2. *Computation of the small scale velocity field $\boldsymbol{u}_s$*

Fung *et al.*[6] wrote the temporal evolution of the small scale structures velocity field $\mathbf{u}_s$ as resulting from the association between advection and decorrelation processes. The velocity field $\mathbf{u}_s$ linked to the small scale vortices is modeled by a modified Billson *et al.*[12] approach. The decorrelation process is mimicked by the following temporal filter:

$$\mathbf{u}_\mathrm{s}(\mathbf{x},t) = a(\mathbf{x})\,\mathbf{v}(\mathbf{x},t) + b(\mathbf{x})\,\boldsymbol{\zeta}(\mathbf{x},t) \tag{7}$$

with $\boldsymbol{\zeta}$, a locally white noise regenerated at each time step with zero statistical mean value in time:

$$\boldsymbol{\zeta}(\mathbf{x}) = 2\sum_{n=N_l+1}^{N} \mathrm{A_n}\cos\left(\mathbf{k}_\mathrm{n}\cdot\mathbf{x}+\varphi_n\right)\boldsymbol{\sigma}_\mathrm{n} \tag{8}$$

In equation (7), the definition of $a = e^{-t/\tau}$ ensures the exponential decorrelation of the velocity field according to a characteristic time scale $\tau = \overline{k}/\varepsilon$. $b = \sqrt{1-a^2}$ allows the conservation of energy in $\overline{k}$ homogenous flows. The advection process of the small scale eddies is taken into account in the computation of $\mathbf{v}$. In the Fung *et al.*[6] study, because of a zero mean velocity field, $\mathbf{u}_s$ was simply advected by the field $\mathbf{u}_l$. Unlike the works of Billson *et al.*[12,13] who resolve an advection equation with the conservative variables for $\mathbf{v}$, it is here considered to be the small scale velocity field at the previous time step advected by the vector field $\mathbf{u}_{bulk} + \mathbf{u}_l$, $\mathbf{u}_{bulk}$ being a velocity vector field. In other words, $\mathbf{v}$ is obtained by solving the advection equation (9):

$$\frac{\partial \mathbf{u}_s(\mathbf{x},t-\Delta t)}{\partial t} + \left(\mathbf{u}_{bulk}(\mathbf{x}) + \mathbf{u}_l(\mathbf{x},t-\Delta t)\right)\cdot\nabla\mathbf{u}_s(\mathbf{x},t-\Delta t) = \mathbf{0} \tag{9}$$

In order to incorporate the mean flow effects in the model, the mean velocity $\overline{\mathbf{U}}$ is chosen for $\mathbf{u}_{bulk}$ in equation (9). One can notice that the validation study for the configuration with $\mathbf{u}_{bulk} = \mathbf{u}_c = 0.6\mathbf{U}_j$ has been done as well. The results will not be presented in the present work.

3. Description of the algorithm numerical implementation

For a detailed explanation of the manner the algorithm works, one resumes the different steps of the method. At each temporal iteration,

- The field $\mathbf{u}_l$ is the first to be generated (equation (5)).
- Once done, the velocity $\mathbf{u}_s^{t-\Delta t}$ linked to the small scale structures at the previous time step is advected by the vector field $(\mathbf{u}_{bulk} + \mathbf{u}_l^{t-\Delta t})$ to obtain $\mathbf{v}$ (equation (9)).
- The white noise $\boldsymbol{\zeta}$ is generated (equation (8)).
- The term $\mathbf{u}_s$ is computed and finally, the turbulent velocity field $\mathbf{u}$ is formed using the equation (1).
- $\mathbf{u}_l$ is stored in order to solve the advection equation (9) at next time step and $\mathbf{u}_s$ is needed to calculate $\mathbf{v}^{t+\Delta t}$.

B. Model validation

For an accurate prediction of the radiated noise outside the jet pump, the formulation must be able to model correctly the acoustic sources inside the tube. Knowing that the behavior of space-time velocity correlations is closely linked to these sources, the model developped in the present work must reproduce precisely statistical aerodynamic quantities such as velocity correlation functions. The velocity correlation coefficient R_{ij} is defined by equation (10):

$$R_{ij}(\boldsymbol{x}, \boldsymbol{r}, \tau) = \frac{\overline{u_i(\boldsymbol{x}, t) u_j(\boldsymbol{x} + \boldsymbol{r}, t + \tau)}}{\sqrt{\overline{u_i(\boldsymbol{x}, t)^2}} \sqrt{\overline{u_j(\boldsymbol{x} + \boldsymbol{r}, t + \tau)^2}}} \tag{10}$$

The model described in subsection A is tested on the Onera Φ80 round circular cold free jet. Many results concerning Φ80 are available at Onera including experiments conducted in CEPRA 19, LES calculations[37] or stochastic methods.[18,20] The nozzle diameter is $D = 80$ mm and the velocity flow U_j is 245 m.s^{-1} $(M = 0.72)$. The evolution of the half velocity diameter $D_{1/2}$ along the jet axis calculated from the steady computation is plotted on the left side in Figure 4. The results show good agreement with experimental data obtained by Fleury *et al.*[33] Radial profiles of the axial mean velocity U for various longitudial positions are given on the right side in Figure 4. The data collapse well with classical hyperbolic tangent profile in the shear layer:

$$\frac{U}{U_a} = 0.5 \left(1 - \tanh \left[\frac{D}{8\delta_\theta} \left(\frac{2y}{D} - \frac{D}{2y} \right) \right] \right) \tag{11}$$

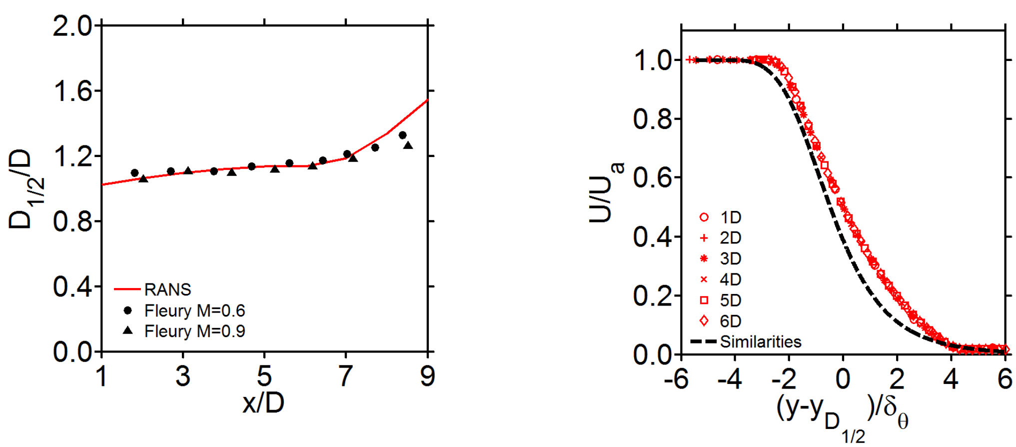

Figure 4. On the left: Evolution of the half velocity diameter $D_{1/2}$ along the $x-$direction. On the right: Radial profiles of the axial mean velocity U for various longitudinal positions compared to the similarity law given in equation (11).

A 2D validation study concerning the velocity correlations in the shear layer is therefore conducted. Validation results are shown for two points located at the center of the shear layer ($y = 0.5D$), as shown in Figure 5.

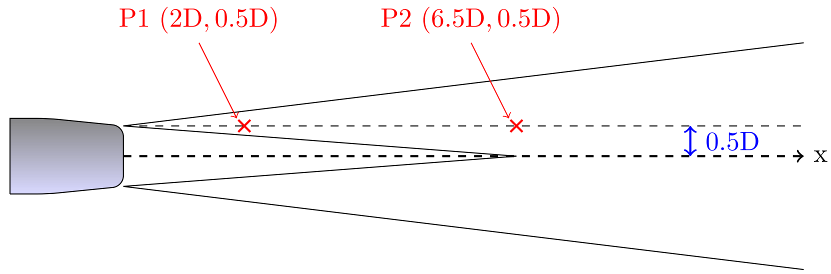

Figure 5. Location of the two points studied in the present work.

For the point P1, a 161×61 points regular cartesian grid is used with $\Delta x = \Delta y = 1$ mm. According to the acoustic dispersion relation $k = \omega/c$, this spatial resolution allows a k_{max} of 1000 m^{-1} so that k_n numbers are picked between 1 and 1000 m^{-1}. For the point P2, a 181×81 points grid is used with $\Delta x = \Delta y = 2$ mm and $1 < k_n < 500$ m^{-1}. The timestep Δt is set to 2.10^{-6}s for P1 against 4.10^{-6}s for P2. In both case, 80 modes are used to discretize the von Kármán-Pao spectra and a simulation consists in 30 000 temporal iterations. An averaging between 10 simulations is done to increase the statistics. Equation (9) is solved using a 6 steps optimized Runge-Kutta algorithm[38] and spatial derivatives are calculated using a 4^{th} order optimized Dispersion-Relation-Preserving scheme. A 10^{th} order filtering is also applied. Results are compared to experimental data obtained by Fleury *et al.*[33] for $M = 0.6$ and 0.9 free jets with a 50 mm nozzle diameter. First, in order to ensure that the "size" of acoustic sources are well estimated, the spatial correlation coefficient $R(x, r, 0)$ is investigated at the point P1. The behaviour of $R(x, r, 0)$ along the line $y = 0.5D$ is plotted on the left in Figure 6. It shows good agreement with experimental results obtained by Fleury *et al.*[33] at M=0.9. R_{11} and R_{22} noticeably reach zero for points distant from P1. This simulation has been repeated at different locations along the $y = 0.5D$ axis between $x = 2D$ and $x = 10D$. The longitudinal integral length scale $L_{11}^{(j)}$ which is defined by

$$L_{11}^{(j)} = \frac{1}{2} \int_{-\infty}^{+\infty} R_{11}(x, x_j, 0) dx_j \tag{12}$$

can be whereas calculated from R_{11} at each longitudinal position. The longitudinal integral length scales $L_{11}^{(1)}$ along the center of the shear layer are plotted on the right in Figure 6. $L_{11}^{(1)}$ are slightly overestimated but its linear growth along the $y = 0.5D$ axis is modeled in a satisfying manner.

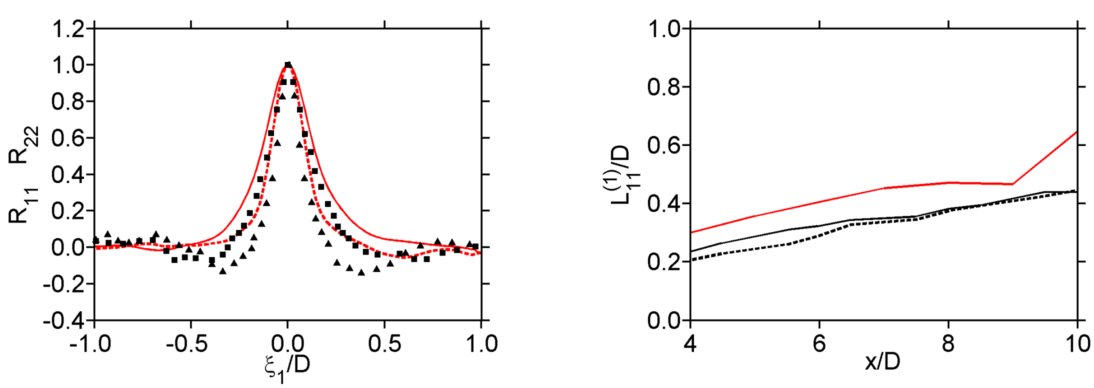

Figure 6. On the left: Present work R_{11}( ) and R_{22} ( ), reference[33] R_{11} (■) and R_{22} (▲). On the right: $L_{11}^{(1)}$ along the center of the shear layer. Present work: ( ). Reference: M=0.6 ( ) and M=0.9 ( ).

At the point P1, correlation functions isocontours are depicted in Figure 7. The size and stretching of R_{11}

and R_{22} patterns are well modeled. The inclination of the isocontours of R_{11}, highlighted by Fleury *et al.*[33] and reported to be a mean flow effect, is well recovered. The principal direction of R_{11} from the axial direction is approximately $\Theta = 19^o$ against $\Theta = 18^o$ in Fleury *et al.*[33] Noticeable numerical errors can arise at the inlet of the domain on both R_{11} and R_{22} isocontour patterns because of the influence of the inlet boundary condition since the extent of the computational domain is pretty small.

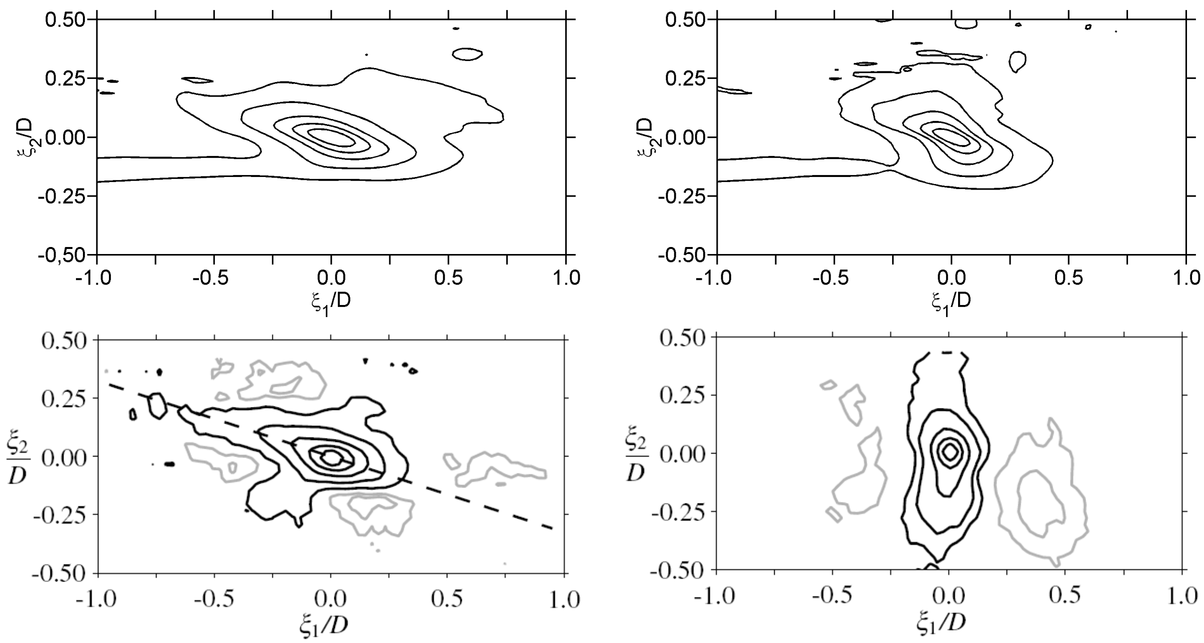

Figure 7. Correlation isocontours at the point P1. $r = \sqrt{\xi_1^2 + \xi_2^2}$**. On the left:** $R_{11}(x, r, 0)$**, plotted levels are (0.05,0.2,0.4,0.6,0.8). On the right:** $R_{22}(x, r, 0)$**, plotted levels are (0.1,0.2,0.4,0.6,0.8). At the top: Present work. At the bottom: Experimental results by Fleury *et al.*[33] at M=0.9 and** $D = 50$**mm.**

Secondly, the space-time velocity correlation functions $R_{ij}(x, r, \tau)$, which is linked to the temporal evolution of the acoustic sources, is studied at the point P2. $R_{11}(\mathrm{x}, \mathrm{r}, \tau)$ patterns are plotted for different values of the time delay τ in Figure 8. The attenuation of $R_{11}(\mathrm{x}, \mathrm{r}, \tau)$ is clearly visible as τ increases. The displacement of the correlation patterns is similar to those found in the experiments.[33] This is corroborated by the left part in Figure 9 where present work results match the experimental curve.[33] The location of the maximum of $R_{11}(\mathrm{x}, \mathrm{r}, \tau)$ according to the time delay τ along the center of the shear layer is well reproduced. Furthermore, the slope of the curve, corresponding to the mean convection velocity of the turbulent structures in the shear layer, is correctly modeled. The right part in Figure 9 shows the time evolution of the longitudinal velocity correlation function R_{11} at P2 with different points located in the shear layer. Similar results have been obtained by Billson *et al.*[12] The attenuation of the correlation function R_{11} with the increasing of r is recovered. This result was expected since $a = e^{-t/\tau}$ in equation (7).

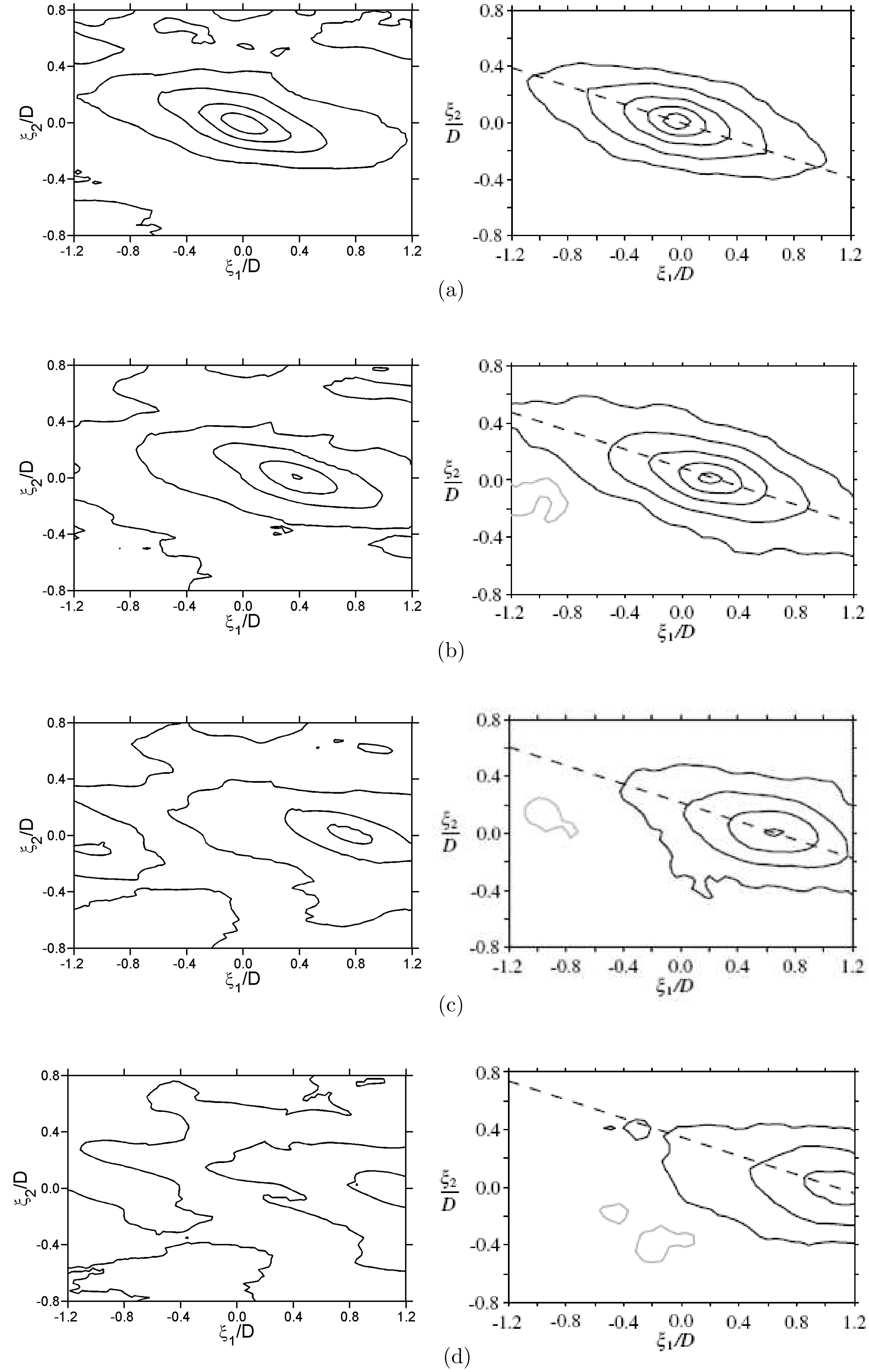

Figure 8. $R_{11}(x, r, \tau)$ patterns at the point P2. On the left: present work at M=0.72. On the right: experimental data obtained by Fleury *et al.*[33] at M=0.9. (a) $\tau = 0$ μs (b) $\tau = 50$ μs (c) $\tau = 150$ μs (d) $\tau = 245$ μs. Isocontours levels are (0.05,0.2,0.4,0.6,0.8).

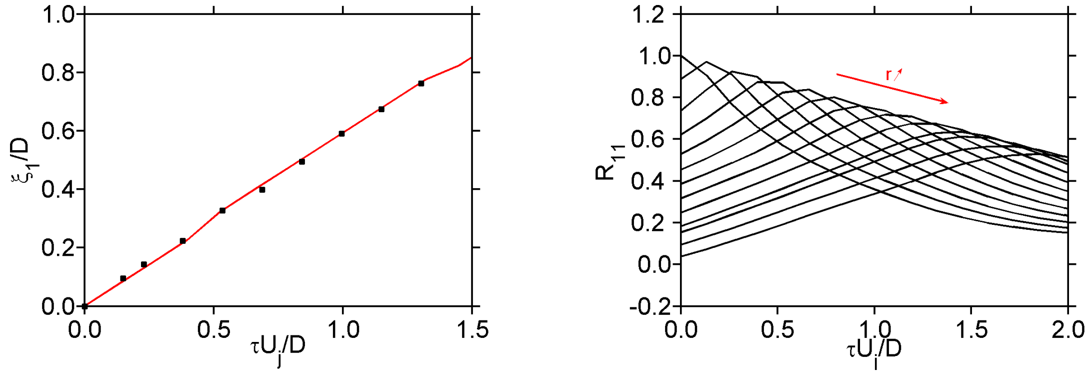

Figure 9. On the left: separation corresponding to the maximum of $R_{11}(x, r, \tau)$ in the convected frame according to the time delay τ. The reference point is P2. Present work (——) and experiments by Fleury *et al.*[33] (■). On the right: $R_{11}(x, r, \tau)$ versus τ for different points located in the shear layer.

The decorrelation of the velocity field is studied at the point P2 too. The attenuation of the correlation functions R_{11} and R_{22} in the center of the shear layer is first investigated in an Eulerian frame on the left in Figure 10. The curves show that R_{11} and R_{22} follow almost the same decorrelation law close to R_{11} attenuation experimental function. Experiments[33] showed more discrepancies between R_{11} and R_{22} decorrelation process. In particular, R_{22} attenuation curve decreases faster than the R_{11} one. This phenomenon is not reproduced by this approach. On the right in Figure 10, the attenuation of the correlation functions in a Lagrangian frame is plotted, i.e $R_{ii}(x, u_c\tau, \tau)$ as a function of τ. Results are in good agreement with experimental data.[33]

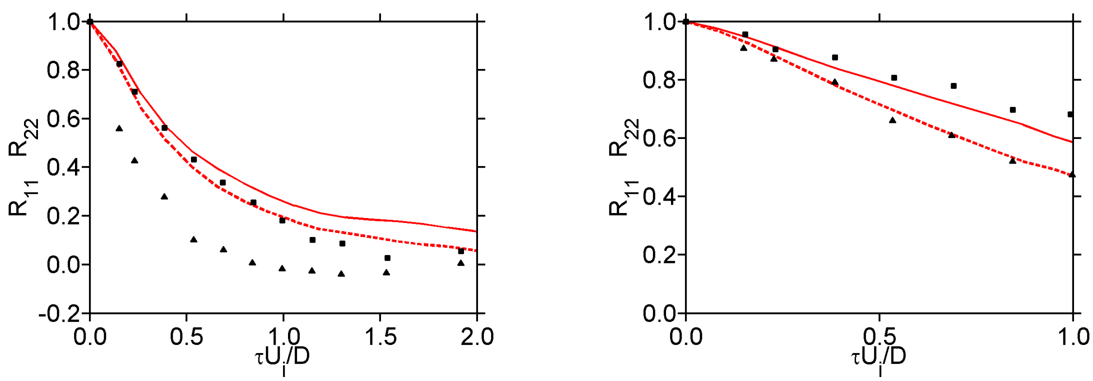

Figure 10. On the left: Eulerian decorrelation of the velocity field at the point P2. On the right: Lagrangian decorrelation of the velocity field at the point P2. Present work: R_{11}(——) and R_{22} (- - -). Reference:[33] R_{11} (■) and R_{22} (▲).

Based on the sweeping hypothesis, the algorithm presented in section A is able to model space-time correlation functions and integral length scales in a satisfying way. Furthermore, the convection velocity of the turbulent structures in the shear layer is correctly taken into account. The mean flow effects are also clearly visible and its influence on velocity correlations is recovered. All these characteristics ensure a satisfying modeling of the acoustic sources "size" and their time evolution. Since the quantities studied in this section are all non-dimensionalized, the reproducibility of the turbulent kinetic energy mapping imposed by the local von Kármaán-Pao spectra must be checked. During a simulation, an energy loss generalized to the whole computational domain is noticeable. Since large scale eddies are built to preserve their part of the energy spectrum, the problem arise from the small scale structures. This loss may be due to the fact that, at each time step, the term $\mathbf{u}_s$ carrying information from upstream points is convected and added to a white noise based on a local von Kármán-Pao spectrum. Despite this issue, it will be shown in section III that the mapping of $\overline{k}$ - and thus the spatial distribution of the most energetic acoustic sources in the jet plume - is not seriously affected.

III. Application to free jet

The method presented in section II is applied to a free jet, the confined configuration being too complex to be considered at first. The simulated jet is the Onera $\Phi 80$ which is a Mach 0.72 cold jet with a nozzle diameter $D = 80$ mm. The $519 \times 108 \times 108$ cartesian grid is shown in Figure 11.

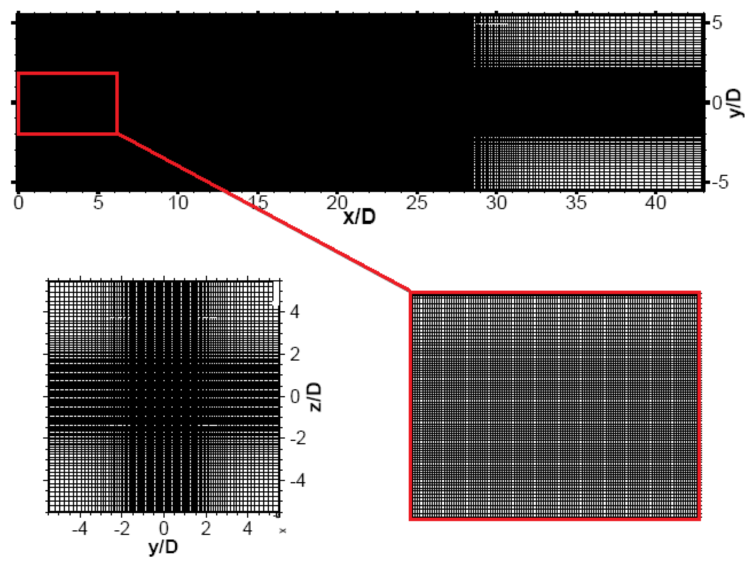

Figure 11. Structure of the 519x108x108 mesh grid.

The domain extends up to $43D$ in the $x-$direction, and is bounded between $-5.5D$ and $5.5D$ in the $y-$ and $z-$directions. In the vicinity of the nozzle exit, edges of the smallest cells are 5 mm long, leading to the ratio $\Delta x/D = 0.0625$. This spatial resolution is held up to $28D$ in the $x-$direction. According to the acoustic dispersion relation, this grid is therefore able to support a k_{max} up to 200 m^{-1} which is a good compromise between the CPU cost and the quality of the aerodynamics modeling in the jet plume. The reproducibility of the results shown in section II using 3-D calculations has been checked. This mesh noticeably allows a satisfying reproduction of the results shown in section II. Nevertheless, one can assume that this spatial resolution will lead to a poor discretization of the von Kármaán-Pao spectra in the vicinity of the nozzle exit since k_{max} has been reduced by a factor 5, from 1000 m^{-1} to 200 m^{-1}. The jet flow conditions are shown in table 1.

Jet exit conditions	
Mach Number	M= 0.72
Diameter	$D = 80$ mm
Pressure	$P = 1013$ hPa
Temperature	$T = 288$ K
Ambient conditions	
Pressure	$P_\infty = 1013$ hPa
Temperature	$T_\infty = 277$ K

Table 1. Flow characteristics

In order to reduce the CPU cost, Omais *et al.*[18] and Gloerfelt *et al.*[34] limited the application of their model to points with a turbulent kinetic energy $\overline{k}$ greater than a preset threshold value. This technique is not applied in our case because of the resolution of the advection equation (9) that imposes to consider all the points in the jet plume. Gloerfelt *et al.*[34] also recommend to smooth the turbulent kinetic energy spatial distribution using a cubic function to avoid discontinuities at the edges of the jet plume. However, their approach is different from that presented in this work, no smoothing of $\overline{k}$ is performed since it leads, because of the resolution of the equation (9), to a stagnation zone at the edges of the jet volume. The model is applied throughout the whole volume, assuming that it will cause a significant increase of the computation cost. The von Kármán-Pao spectrum is discretized linearly by 100 modes picked between $k_1 = 2$ m^{-1} and $k_{max} = 200$m^{-1}. A damping zone is set from $x = 28D$ to the end of the domain in order to avoid spurious waves that could contaminate the solution. A stretching of the mesh in the downstream direction is applied in this region to improve efficiency of the artificial numerical dissipation. The simulation is performed during 4000 iterations with a time step $\Delta t = 8 \cdot 10^{-6}$ s. It tooks 24 CPU hours on a NEC SX-8 supercomputer to generate the stochastic field.

1. *Aerodynamic results*

A snapshot of each synthetized velocity components is given in Figure 12 for a given time. The vector field **u** in the $x-y$ median plane is shown in Figure 16.

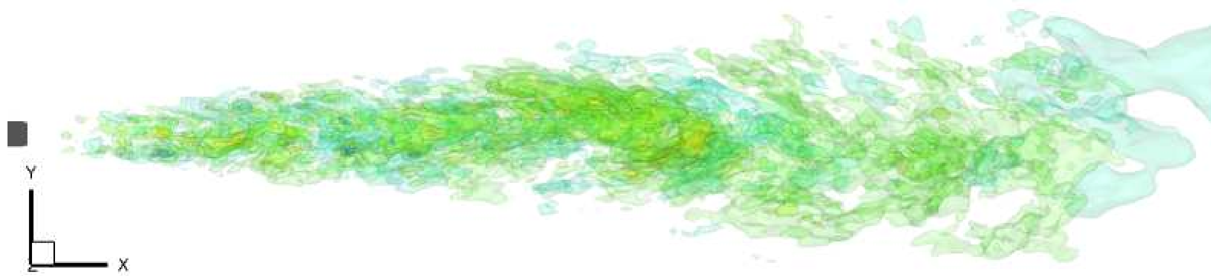

(a)

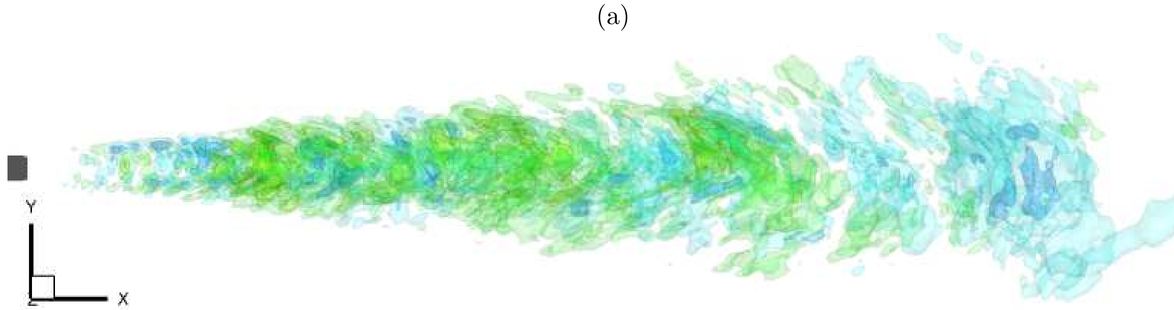

(b)

Figure 12. Isocontours of synthetic velocity (u) components in the $x-y$ plane after 3000 iterations (t=0.024s, structures moving at $\mathrm{u}_c = 0.6\mathrm{U}_j$ covered $44.1D$ in the longitudinal direction). (a) u, (b) v. Levels are (-50,-40,-30,-20,20,30,40,50) m.s^{-1}.

The effects of the mean flow are clearly visible in particular in the zone located right after the end of the potential core. It is also visible regarding the snapshot of the Q criterion in the $x-y$ median plane presented in Figure 13. Growing turbulent structures exist everywhere in the jet plume. Radial profiles of u_{RMS} and v_{RMS} are compared to data obtained by Fleury *et al.*[33] for cold free jets at $M = 0.6$ and $M = 0.9$ in Figure 14. In the present work, turbulence intensities levels are lower in comparison with the reference results.[33] Noticeably, it reaches zero in the potential core. Nevertheless, these discrepancies were expected since a loss of energy occurs during the transition from $\overline{k}_{RANS}$ to the turbulent kinetic energy supported by the grid. If the profile located at $x = 4D$ and $x = 5D$ are almost superimposed, turbulence intensities at $x = 2D$ and $x = 3D$ do not follow the law of similarity. This phenomenon is due to the spatial resolution of the grid: at these points, a relatively larger part of the von Kármaán-Pao spectra lies beyond k_{max}. Then, the anisotropy showed by the experimental data is not mimicked by the model. The same observation can be done regarding Figure 15 representing the evolution of turbulence intensities along the jet axis. Nevertheless, the general behaviour of the curves is well modeled.

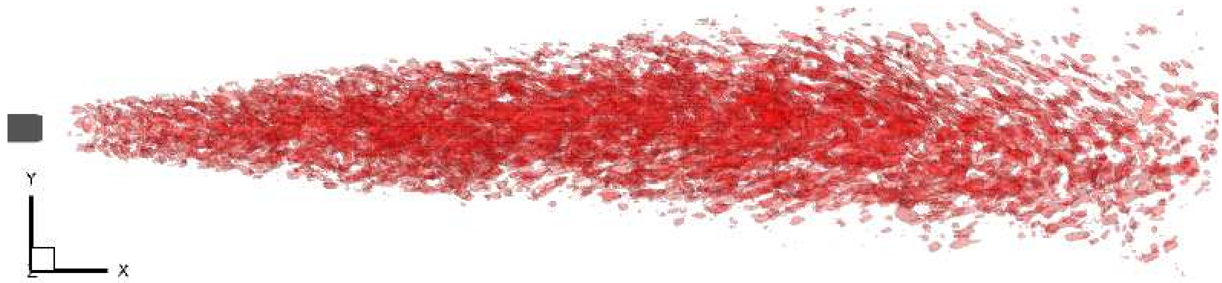

Figure 13. Instantaneous Q criterion isocontour in the x-y median plane after 3000 iterations (t=0.024s, structures moving at $u_c = 0.6U_j$ covered $44.1D$ in the longitudinal direction). Level is $Q_c = -5.10^5 s^{-2}$.

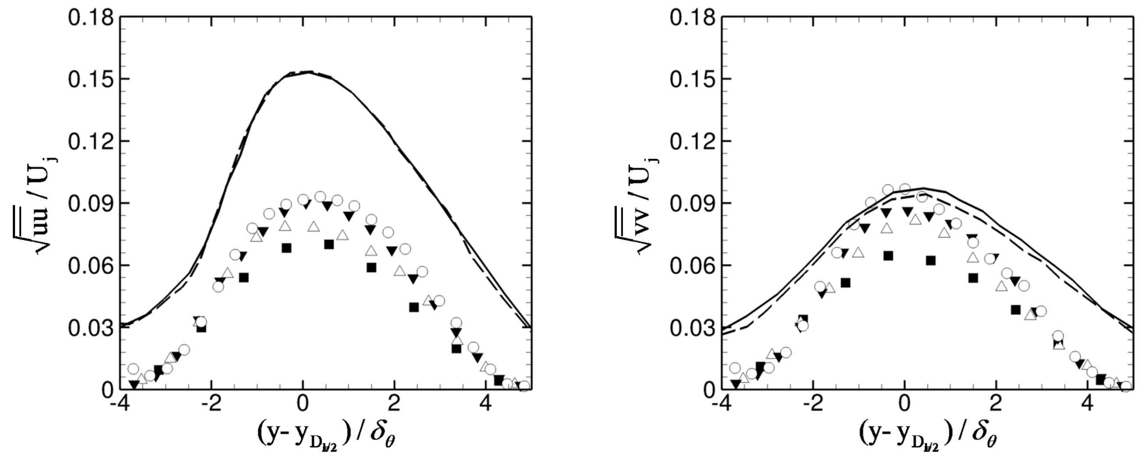

Figure 14. On the left: $\sqrt{\overline{uu}}/U_j$, on the right: $\sqrt{\overline{vv}}/U_j$. Present work: radial profile at $x = 2D$ (■), $x = 3D$ (△), $x = 4D$ (▽), $x = 5D$ (○). Reference:[33] profile of the turbulence intensities averaged between $x = 2D$ to $x = 5D$ for a cold free jet at M$= 0.6$ (━━) and M$= 0.9$ (- - -)

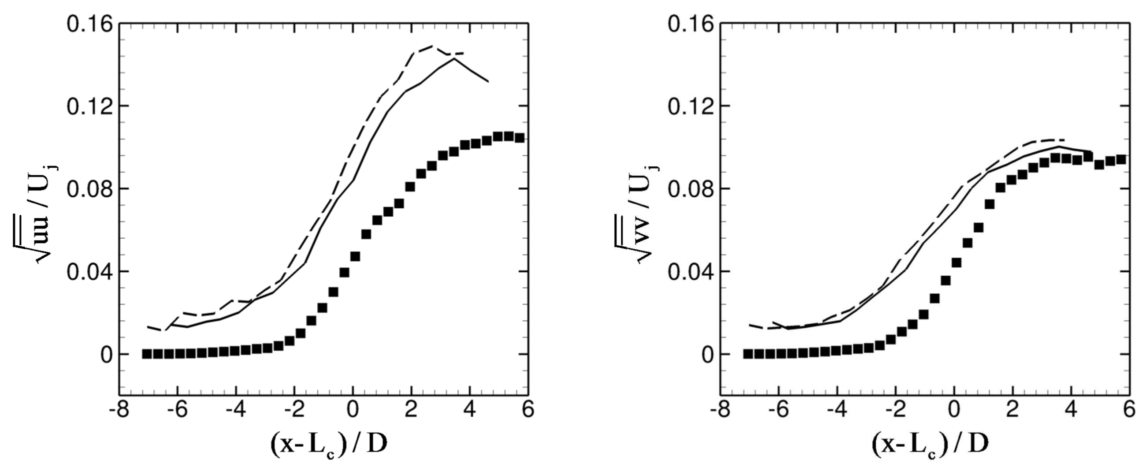

Figure 15. Longitudinal profile of the turbulence intensities along the jet axis. On the left: $\sqrt{\overline{uu}}$, on the right: $\sqrt{\overline{vv}}$. Present work (■), reference:[33] M$= 0.6$ (━━), M$= 0.9$ (- - -).

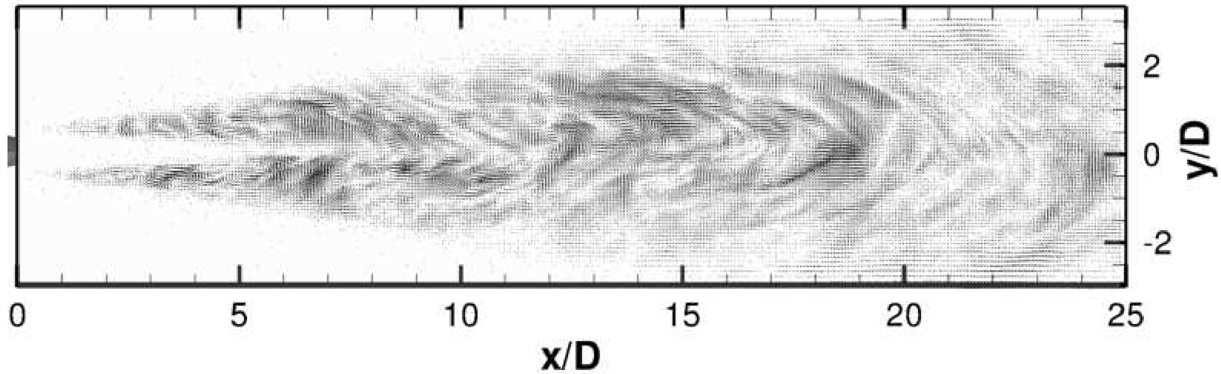

Figure 16. Velocity vector field in the x-y median plane.

A snapshot of the velocity vector field in the x-y median plane is shown in Figure 16 for a given time ($t = 0.024$ s). The effects of the mean flow are clearly visible. This field is similar to that obtained by Billson *et al.*[12] The apparent isotropy of the stochastic velocity field observed in Figure 14 and 15 is verified in Figure 17 where the power spectral densities of each components u, v, w are plotted for different locations in the center of the shear layer between $x = 2D$ and $x = 7D$. The turbulent velocity field is reported to be isotropic at the center of the shear layer since each component has the same spectral content. Following the former idea of Smirnov *et al.*,[15] Billson *et al.*[13] proposed a method to take the turbulence anisotropy into account. Anyway, recent studies[19,18] showed that anisotropy had little effects on the acoustic radiation of cold free jets. In Figure 17, the energy linked to the "low frequencies" logically increases with the longitudinal position x. For points located downstream of $x = 4D$, one can notice a slight inflection of the spectra around $St = 1.5$. For these points, k_e is small so that the von Kármán-Pao energy spectrum is centered on the low wavenumbers. Nevertheless, a high number of modes are used to discretize the "small scale" part of the spectrum even if there is few $\overline{k}$ to inject in the wave number space. This inflection might be due to the fact that there is no transition between "large" and "small" scale modes.

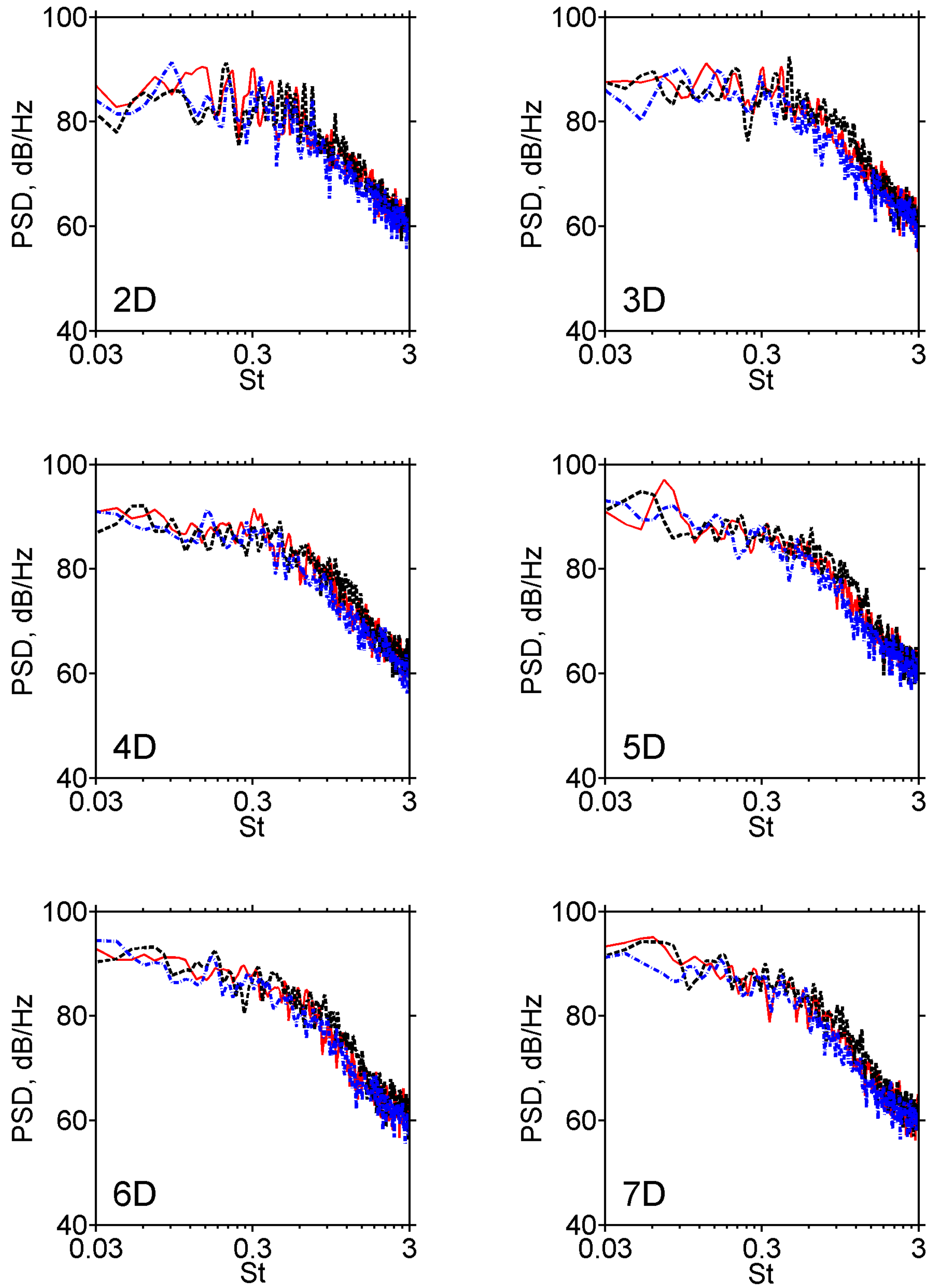

Figure 17. Power spectral density of u (▬▬), v (- - -) and w (- - -) for different longitudinal positions at the center of the shear layer.

A mapping of the reconstructed turbulent kinetic energy $1/2(\overline{u^2} + \overline{v^2} + \overline{w^2})$ is compared to that injected from the von Kármán-Pao spectrum in Figure 18. There are noticeable discrepancies between this two fields. First, a part of turbulent kinetic energy has been lost during the calculation. Secondly, in the simulation, the energetic zone located downstream of the end of the potential core extends further downstream.
Nevertheless, the method is able to reproduce the two 'energetic lobes' located in the shear layer. This is corroborated by the turbulent kinetic energy $\overline{k}$ profiles plotted in Figure 19. The evolution of $\overline{k}$ along the $y = 0.5D$ axis is shown on the left in Figure 19. One can notice that the longitudinal position corresponding

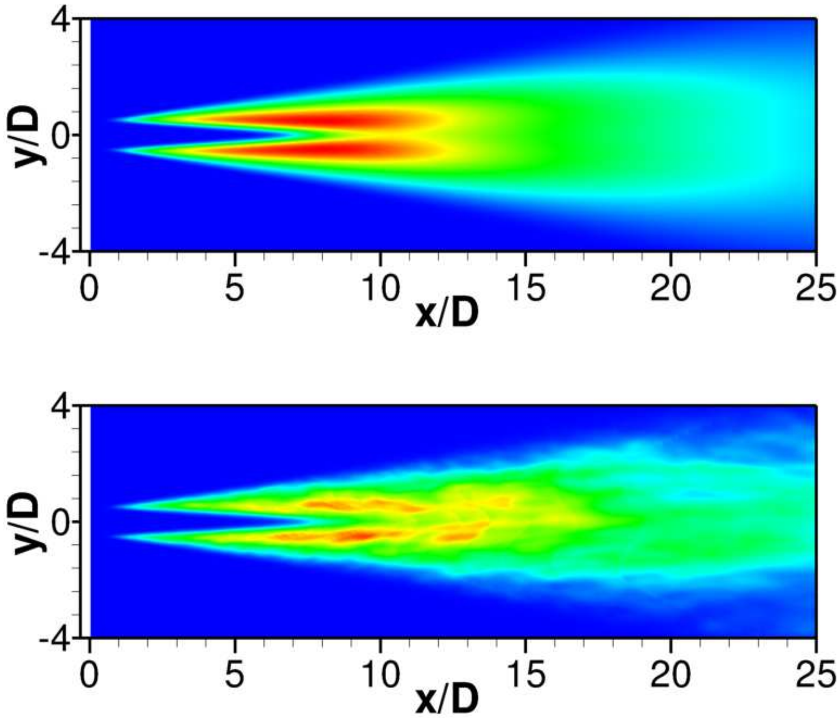

Figure 18. Turbulent kinetic energy $\overline{k}$ mapping. At the top: injected from the von Kármán-Pao spectra, at the bottom: reconstructed from the stochastic field by averaging over 4000 temporal iterations. Levels are taken between 0 and 1200 m^2/s^2.

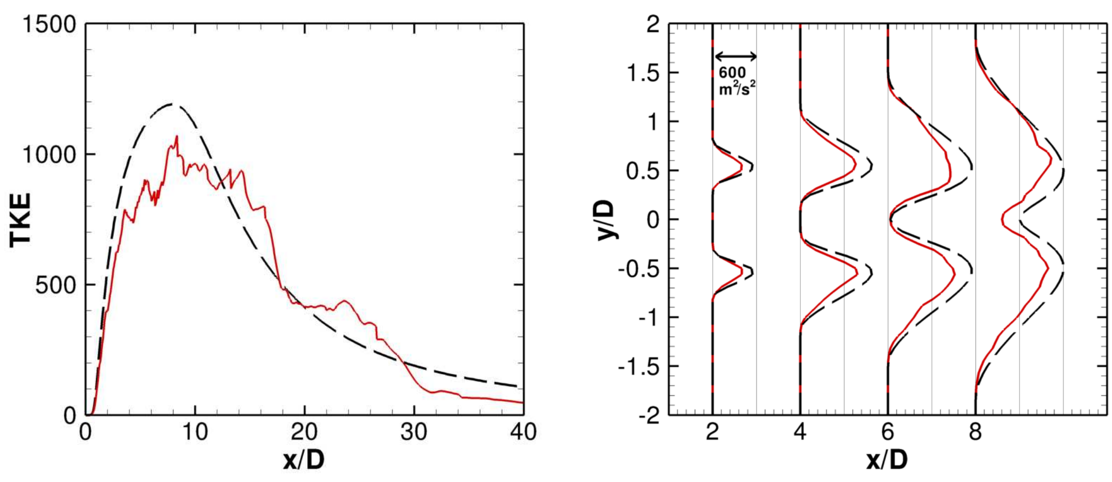

Figure 19. On the left: turbulent kinetic energy $\overline{k}$ along the axis $y = 0.5D$. On the right: turbulent kinetic energy radial profile at different longitudinal positions. TKE reconstructed from the present work by averaging over 4000 temporal iterations ( ) and imposed by the von Kármaán-Pao spectra ( ).

to the maximum of energy is well modeled. The radial profiles of $\overline{k}$ at different longitudinal positions are plotted on the right in Figure 19. Despite the loss of energy, the radial evolution of the turbulent kinetic energy at each location is mimicked in a satisfying way. Therefore, the turbulent kinetic energy map initially imposed by the von Kármaán-Pao spectra is not highly affected so that the spatial distribution of the most energetic acoustic sources is preserved. Nevertheless, some studies are still ongoing to remedy the energy loss issue. One can remark that for an energy conserving method, $\overline{\mathbf{u}^2}$ should locally follow the relation:

$$\frac{1}{2}\overline{\mathbf{u}^2} = \sum_{k=1}^{N} E(k)dk$$

Decomposing $\mathbf{u}$, the term $0.5\overline{\mathbf{u}_l^2}$ should reproduce - as it is the case - the "large scale" part of the von Kármán spectrum. On the other hand, the term $0.5\overline{\mathbf{u}_s^2}$ should reproduce the part allowed to the "small scale" structures. It has been shown in section II that a loss of energy is clearly linked to this term. An attempt to renormalize $\mathbf{u}_s$ at each time step using the amplitude of $\boldsymbol{\zeta}$, built with the local von Kármán-Pao spectra has been done. It allowed to reproduce the mapping of $\overline{k}$ avoiding the loss of energy. But because the correction was dependent on space, it caused the decorrelation of the velocity field. In addition, $\overline{\mathbf{u}_l\mathbf{u}_s}$ should be logically equal to zero. Naturally, it is not the case since $\mathbf{u}_l$ participates to the advection of $\mathbf{u}_s$. Nevertheless, the energy linked to the term $\overline{\mathbf{u}_l\mathbf{u}_s}$ is clearly negligible.

2. *Far field acoustic results*

Acoustic radiation in the far field is computed using the temporal formulation of the Lighthill analogy. Source terms are therefore directly obtained from the synthetic velocity field. The entropy source terms are neglected since the jet is isothermal.

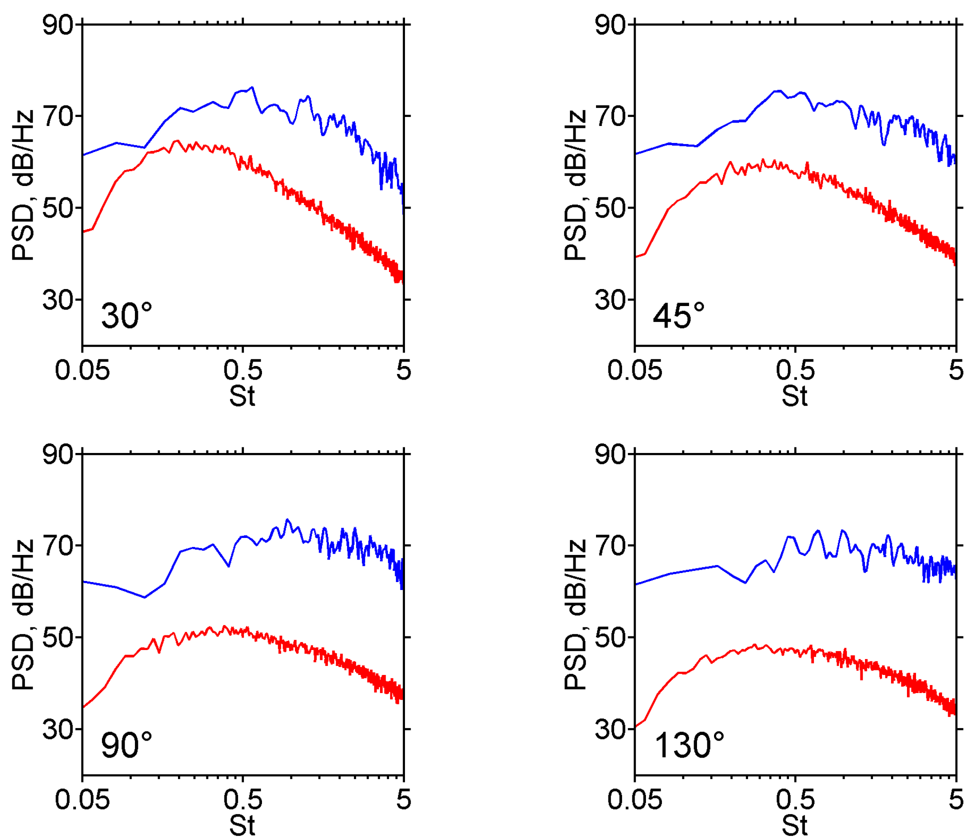

Figure 20. Power spectral density of far field pressure signals for different angles: Present work (blue line) and experiments (red line).

The source domain is smoothed via a cubic function in order to force source terms to reach zero at the boundaries of the domain. The results are compared with Onera experimental data for the Φ80 free jet. The far field spectra are computed for four observers located at 75 diameters from the nozzle exit. Respective angles of the observers are 30^o, 45^o, 90^o and 130^o from the jet axis. The curves are plotted in Figure 20. The global shapes of the simulated spectra are reproduced in a satisfying manner. In particular, the slope at "high frequencies" of the acoustic spectra for observers located at 30^o and 45^o are in good agreement with those of the experiments. A shift in amplitude occurs at every angle and increases from 15 dB at 30^o to 30 dB at 130^o. A similar shift has already been reported by Billson *et al.*[12] for an observer located at 30^o in the far field of a M=0.75 free jet with the calibration factor α_f set to 1.
However, the peak frequency is overestimated on average by a factor 2. A similar issue has been reported previously.[12,13,18] In this case, it could be linked to the average of the dissipation rate $< \varepsilon >$ used to compute Kolmogorov pulsations ω_n using equation (6). This could also be linked to the way the Doppler effect is reproduced by the model. Even if the method developed in the present work is able to reproduce the "energetic lobes" which characterize a typical subsonic jet's turbulent kinetic energy mapping, one can notice that the zone where the maximum of energy is injected from the von Kármaán-Pao energy spectra is slightly displaced downstream in comparison with the most energetic points mapping given by the steady calculation. In addition, because of the spatial resolution and the choice of k_{max}, there is no turbulence in the vicinity of the nozzle. Thus, even if the spatial distribution of the most energetic acoustic sources is not highly affected, it differs from that given by the RANS solution. Consequently, the doppler effect which is linked in this case to the advection of the acoustic source terms in the jet plume could not be exactly mimicked.

IV. Conclusions and perspective

The present work is a first step towards the development of a predictive tool for aeroacoustics. The stochastic method designed to build the acoustic sources is more specifically presented in this paper. Starting from a steady RANS computation, it is able to generate an isotropic and homogenous turbulent velocity field reproducing faithfully statistical aerodynamic quantities in the flow. This turbulent field is then used to calculate acoustic source terms to be introduced in the acoustic propagation equations. The final goal of this study is to develop a tool for acoustics of confined jets. This configuration being too complex to be studied at first, the model has been tested on a cold free jet. Following the former idea of Fung *et al.*[6] and the work of Siefert and Ewert,[25] the model is based on the sweeping hypothesis which is known to be of major importance in the velocity decorrelation mechanism. The expressions of velocities linked to larger and smaller scale structures have been build following respectively a Bailly and Juvé[11] method and a modified Billson *et al.*[12] formulation.
To make sure, acoustic source terms are correctly modeled inside the tube, the method has been validated on its ability to reproduce statistical aerodynamic quantities such as velocity correlations. The results are satisfactory in 2-D and 3-D. Noticeably, integral length scales, effect of the mean flow and convection of the turbulent structures are modeled in a satisfying way. An issue remains in the formulation concerning turbulent kinetic energy preservation. Studies are still ongoing to solve this problem. Acoustic spectra are overestimated approximately by 15dB and a shift in frequency occurs. Noticeably, the global behaviour of the curves at all angles are in good agreement with the experiments and in particular the slope of spectra at high frequencies.
The next step is to apply the method to the confined case. The validated model will be used inside the tube to compute the acoustic source terms to inject in the Euler's equations. These equations will allow us to model the propagation of sound in the flow. Once in the far field outside the tube, the Kirchoff analogy will be used to recover pressure signals at the observers. The final tool will be validated by comparing numerical results with data previously obtained from an experimental campaign including LDV measurements inside the tube and far-field acoustic acquisitions.

References

[1]Tam, C. and Auriault, L., "Jet mixing noise from fine-scale turbulence," *AIAA Journal*, Vol. 37, No. 2, 1999, pp. 145–153.
[2]Kraichnan, R., "Diffusion by a random velocity field," *Phys. Fluids*, Vol. 13, 1970, pp. 22–31.
[3]Favier, B., Godeferd, F., and Cambon, C., "On space and time correlations of isotropic and rotating turbulence," *Phys. Fluids*, Vol. 22, 2010.

[4]Osborne, D., Vassilicos, J., Sung, K., and Haigh, J., "Fundamentals of pair diffusion in kinematic simulations of turbulence," *Physical Review E*, Vol. 74, 2006.

[5]Thomson, D. and Devenish, B., "Particle pair separation in kinematic simulations," *J. Fluid Mech.*, Vol. 526, 2005, pp. 277–302.

[6]Fung, J., Hunt, J., Malik, N., and Perkins, R., "Kinematic Simulation of Homogeneous Turbulence by Unsteady Random Fourier Modes," *J. Fluid Mech.*, Vol. 236, 1992, pp. 281–318.

[7]Fung, J. and Vassilicos, J., "Kinematics Simulation of Homogeneous Turbulence by Unsteady Random Fourier Modes," *Physical Review E*, Vol. 57, 1998, pp. 1677.

[8]Karweit, M., Blanc-Benon, P., Juvé, D., and Comte-Bellot, G., "Simulation of the propagation of an acoustic wave through a turbulent velocity field : a study of phase variance," *J. Acoust. Soc. Am.*, Vol. 89, No. 1, 1991, pp. 52–62.

[9]Bechara, W., Bailly, C., Lafon, P., and Candel, S., "Stochastic approach to noise modeling for free turbulent flows," *AIAA Journal*, Vol. 32, No. 3, 1994, pp. 455–463.

[10]Bailly, C., Lafon, P., and Candel, S., "A stochastic approach to compute noise generation and radiation of free turbulent flows," *1st AIAA/CEAS Aeroacoustics Conference, AIAA Paper 99-1872*, Munich, Germany, 12-15 June 1995.

[11]Bailly, C. and Juvé, D., "A stochastic approach to compute subsonic noise using linearized Euler's equations," *5th AIAA/CEAS Aeroacoustics Conference, AIAA Paper 99-1872*, Seattle, Washington, 10-12 May 1999.

[12]Billson, M., Eriksson, L., and Davidson, L., "Jet noise prediction using stochastic turbulence modeling," *9th AIAA/CEAS Aeroacoustics Conference, AIAA Paper 2003-3282*, Hilton Head, South Carolina, 12-14 May 2003.

[13]Billson, M., Eriksson, L., Davidson, L., and Jordan, P., "Modeling of synthetic anisotropic turbulence and its sound emission," *10th AIAA/CEAS Aeroacoustics Conference, AIAA Paper 2004-2858*, Manchester, England, 10-12 May 2004.

[14]Billson, M., Eriksson, L., and Davidson, L., "Jet noise modeling using synthetic anisotropic turbulence," *10th AIAA/CEAS Aeroacoustics Conference, AIAA Paper 2004-2858*, Manchester, England, 10-12 May 2004.

[15]Smirnov, A., Shi, S., and Celik, I., "Random flow generation technique for large eddy simulations and particle-dynamics modeling," *ASME Journal of Fluids Engineering*, Vol. 123, 2001, pp. 359–371.

[16]Snellen, M., Van Lier, L., Golliard, J., and Védy, E., "Prediction of the flow induced noise for practical applications using the SNGR method," *Tenth International Congress on Sound and Vibration*, Stockholm, Sweden, 7-10 July 2003.

[17]Casalino, D. and Barbarino, M., "A stochastic method for airfoil self-noise computation in frequency-domain," *16th AIAA/CEAS Aeroacoustics Conference, AIAA Paper 2010-3884*, Stockholm, Sweden, 7-9 June 2010.

[18]Omais, M., Caruelle, B., Redonnet, S., Manoha, E., and Sagaut, P., "Jet noise prediction using RANS CFD input," *5th AIAA/CEAS Aeroacoustics Conference, AIAA Paper 2008-2938*, Vancouver, Canada, 5-7 May 2008.

[19]Dembinska, F., *Modélisation stochastique des sources acoustiques générées par la turbulence : application au bruit de jet*, Ph.D. thesis, Universit Pierre et Marie Curie, 2009.

[20]Le Garrec, T., Manoha, E., and Redonnet, S., "Flow noise predictions using RANS/CAA computations," *16th AIAA/CEAS Aeroacoustics conference*, Stockholm, Sweden, 7-9 June 2010.

[21]Careta, A., Sagus, F., and Sancho, J., "Stochastic generation of homogenous isotropic turbulence with well-defined spectra," *Physical Review E*, Vol. 48, No. 3, 1993, pp. 2279–2287.

[22]Ewert, R. and Edmunds, R., "CAA slat noise studies applying stochastic sound sources based on solenoidal filters," *11th AIAA/CEAS Aeroacoustics Conference, AIAA Paper 2005-2862*, Monterrey, California, 23-25 May 2005.

[23]Ewert, R., "Broadband slat noise prediction based on CAA and stochastic sound sources from a fast Random Particle-Mesh (RPM) method," *Computers and Fluids*, Vol. 37, 2008, pp. 369–387.

[24]Ewert, R., Dierke, J., Pott-Pollenske, M., Appel, C., Edmunds, R., and Sutcliffe, M., "CAA-RPM prediction and validation of slat setting influence on broadband high-lift noise generation," *16th AIAA/CEAS Aeroacoustics Conference, AIAA Paper 2010-3883*, Stockholm, Sweden, 7-9 June 2010.

[25]Siefert, M. and Ewert, R., "Sweeping sound generation in jets realized with a random particle-mesh method," *15th AIAA/CEAS Aeroacoustics Conference, AIAA Paper 2009-3369*, Miami, Florida, 11-13 May 2009.

[26]Dieste, M. and Gabard, G., "Synthetic turbulence applied to broadband interaction noise," *15th AIAA/CEAS Aeroacoustics Conference, AIAA Paper 2009-3267*, Miami, Florida, 11-13th May 2009.

[27]Dieste, M. and Gabard, G., "Random-vortex-particle methods for broadband fan interaction noise," *16th AIAA/CEAS Aeroacoustics Conference, AIAA Paper 2010-3885*, Stockholm, Sweden, 7-9 June 2010.

[28]Lee, S., Lele, S., and Moin, P., "Simulation of spatially evolving turbulence and the applicability of Taylor's hypothesis in compressible flow," *Phys. Fluids A*, Vol. 4, No. 7, 1992, pp. 1521–1530.

[29]Jarrin, N., Benhamadouche, S., Laurence, D., and Prosser, R., "A synthetic-eddy-method for generating inflow conditions for large-eddy simulation," *International Journal of Heat and Fluid Flow*, Vol. 27, No. 4, 2006, pp. 585–593.

[30]Jarrin, N., Prosser, R., Uribe, J., Benhamadouche, S., and Laurence, D., "Reconstruction of turbulent fluctuations for hybrid RANS/LES simulations using a synthetic-Eddy Method," *International Journal of Heat and Fluid Flow*, Vol. 30, No. 3, 2009, pp. 435–442.

[31]Rubinstein, R. and Zhou, Y., "Time correlations and the frequency spectrum of sound radiated by turbulent flows," Tech. rep., NASA contract., 1997, NAS1-19480.

[32]Rubinstein, R. and Zhou, Y., "The frequency spectrum of sound radiated by isotropic turbulence," *Phys. Lett. A*, Vol. 267, 2000, pp. 379–383.

[33]Fleury, V., Bailly, C., Jondeau, E., Michard, M., and Juvé, D., "Space-time correlations in two subsonic jets using dual particle image velocimetry measurements," *AIAA Journal*, Vol. 46, No. 10, 2008, pp. 2498–2509.

[34]Gloerfelt, X., Bailly, C., and Bogey, C., "Full 3-D application of the SNGR method to isothermal Mach 0.9 jet," Tech. rep., JEAN project, 2003.

[35]Bailly, C., Gloerfelt, X., and Bogey, C., "Report on stochastic noise source modelling," Tech. rep., Projet JEAN, 2002.

[36]Batten, P., Goldberg, U., and Chakravarthy, S., "Reconstructed sub-grid methods for acoustic predictions at all Reynolds numbers," *8th AIAA/CEAS Aeroacoustics Conference, AIAA Paper 2002-2511*, Breckenridge, Colorado, 17-19th June 2002.

[37]Muller, F., *Simulation de jets propulsifs: application à l'identification de phénomènes générateurs de bruit*, Ph.D. thesis, Numerical Simulation and Aeroacoustic Dept., ONERA, Châtillon, 2006.

[38]Bogey, C. and Bailly, C., "A family of low dispersive and low dissipative explicit schemes and noise computations," *J. Comput. Phys.*, Vol. 194, 2004, pp. 194–214.